Dynamics of Continuous, Discrete and Impulsive Systems
Series **B:** *Applications & Algorithms* **25 (2018)** 181-196

EXTENDING SIMPLE MODELS OF SWIMMING PLANKTON: NONLINEARITY, TRANSPORT, AND IRREGULAR ORBITS

Marek Stastna[1], Justin Shaw [1], Michael Waite[1]

[1]Department of Applied Mathematics
University of Waterloo, Waterloo, Ontario N2L 3G1, Canada

Abstract. We study the dynamics of shear triggered swimming plankton in simple hydrodynamic flows of increasing complexity building on the classical solution due to Stokes for a viscous half space above an oscillating plate. Even though the Navier-Stokes equations that govern fluid flow linearize in this situation, the plankton, or Lagrangian, response is nonlinear. We characterize both the Eulerian response and the nonlinear Lagrangian response. The Eulerian analysis demonstrates that there is a cut-off swimming velocity below which no periodic behaviour is possible. The precise value of the cutoff depends on the amplitude of the harmonic driving. The Lagrangian analysis demonstrates that for commensurate frequencies a net horizontal transport is possible, while for incommensurate frequencies the spectrum of the motion exhibits a systematic increase of high frequency components and in some cases very complex phase space behaviour. Nevertheless, the phase portraits for varying initial conditions remain translations of one another implying that no chaotic behaviour results. Finally, we demonstrate that in striking contrast to the Lagrnagian analysis, Eulerian analysis does not discriminate between perturbations with commensurate and incommensurate frequency.

Keywords. zooplankton locomotion, ordinary differential equations, hydrodynamics, nonlinear dynamics, individual based models, rheotaxis, transport.

AMS (MOS) subject classification: 92B01

1 Introduction

Nonlinear phenomena can arise from a biological response to linear flows. In the accompanying paper we have discussed how the flee response of swimming plankton, triggered by either shear or acceleration of the ambient fluid exceeding a critical value, yields a limit cycle response. We have also outlined a simple experiment, inspired by classical techniques in rheology [9], that allows for the discrimination between a shear triggered or acceleration triggered response for a particular plankton species. See [3] for field measurements which inspired these investigations, and [8] for related modelling of a shear response.

In this manuscript we further explore the nonlinearities introduced by the plankton's ability to swim. The results are extended beyond the simplest limit cycles introduced in the accompanying paper by exploring the effects of multiple driving frequencies. The Eulerian flow for the simple configuration of a viscous fluid above an oscillating plate is linear, yielding the superposition of the solution for each driving frequency [5]. This retains the decoupling of plankton motion into driving by flow in the horizontal direction, and swimming and sinking in the vertical direction, but increases the complexity of the driving.

The swimming plankton problem is a modification of the Lagrangian fluid particle problem. It is not linear in even the simplest case, with further complications introduced when inertia is considered [1]. In this manuscript we consider the case of a primary driving frequency with one perturbation. The nature of the particle paths in the two driving frequency case depends on whether or not the frequencies are commensurate as well as the strength of the perturbation driving frequency. When the two driving frequencies are commensurate we demonstrate that the symmetry necessary for the limit cycle is broken and a net horizontal transport results. In contrast, when the two frequencies are incommensurate, the symmetry breaking of the limit cycle is more complex. In many cases this yields a "smeared" limit cycle, but we also explicitly demonstrate an instance of very complex phase space behaviour that bears little resemblance to the basic limit cycle solution.

To quantify how the amplitude of the perturbation driving frequency influences the region of phase space that the response covers we use a tiling algorithm we call the "tiling fraction." We find that perturbation frequencies that are lower than the primary driving frequency yield the largest increase in tiling fraction; in some cases reaching approximately 0.5. When the tiling fraction is plotted as a function of the amplitude of the forcing, the resulting curve is not monotonic: the primary forcing is assumed to have an amplitude of 1, and when perturbation amplitudes are larger than 0.4 there is a decrease in tiling fraction.

We also examine Eulerian transport, demonstrating that while the Lagrangian analysis is qualitatively different for the cases of commensurate and incommensurate driving frequencies, the transport is essentially unchanged.

The results presented provide a concrete example of how even simple biological responses to hydrodynamic cues may greatly effect Lagrangian particle motion.

2 Methods

The basic motion of the fluid above the oscillating plate is described by the same simplification of the Navier Stokes equations as in the accompanying paper. The only non-zero component of the velocity field is given by

$$u(z,t) = U_0 \cos(\omega t - mz)\exp(-mz), \tag{1}$$

while the vertical component is zero. Here

$$m = \sqrt{\frac{\omega}{2\nu}}. \tag{2}$$

where ν is the kinematic viscosity. It can be seen that the vertical decay scale of motion ($L_d = 1/m$) and vertical period of oscillation ($L_o = 2\pi/m$) scale with the square root of viscosity, and the square root of the period of oscillation $T_p = 2\pi/\omega$. When the plate's motion is a combination of two frequencies $u(0,t) = \cos(\omega t) + a_2 \cos(\omega_2 t)$ the motion will be a superposition of two profiles of the form (1) due to the linearity of the geometrically reduced Navier Stokes equations.

By analogy with the definition of a field line, the motion of the particles can be expressed as

$$\frac{d\vec{x}}{dt} = \vec{u}_{\text{fluid}}(x(t), z(t), t) + \vec{u}_{\text{particle}}(x(t), z(t), t) \tag{3}$$

which for our situation simplifies to

$$\frac{d\vec{x}}{dt} = [u(z(t),t), 0] + [0, w_{\text{sink}} + H(|u_z(z(t),t)| - u_z^{\text{critical}})w_{\text{swim}}]. \tag{4}$$

In the accompanying manuscript we have discussed the design of experiments that can determine whether swimming is triggered by shear or acceleration. As in this previous work, we choose w_{sink} to be a constant and model the triggered response using a Heaviside function: if the value of the flow parameter is higher than the critical value u_z^{critical} the particles swim up. We thus have a swimming behaviour that acts only in the vertical direction and a flow which acts only in the horizontal direction. This is the simplest nontrivial coupling of these two mechanisms and will be referred to as the Lagrangian model. In the text below, the various formulae will be presented with a shear triggered swimming behaviour.

Even the Lagrangian model, which is the simplest form of nontrivial coupling between the fluid dynamics and particle swimming, has an explicit time dependence in the right hand side of the differential equations for the particle position. This means that much of the intuition from the study of autonomous differential equations does not apply. However, due to the simplicity of the system a relatively simple Eulerian analysis can be carried out. The first point to note is that both the fluid flow and the swimming behaviour have no explicit x dependence and hence the phase space behaviour is translation invariant in the horizontal direction. At each z the cumulative vertical transport can be defined as

$$W_{\mathrm{cum}}(z,t) = \int_0^t \left[-w_{\mathrm{sink}} + w_{\mathrm{swim}} H(|u_z(z(s),s)| - u_z^{\mathrm{critical}})\right] ds. \tag{5}$$

This expression is meaningful regardless of whether the motion of the underlying plate that drives the motion is taken to be a single frequency or a combination of multiple frequencies. However, when there is a single driving frequency T may be taken to be the period. Similarly when there are multiple driving frequencies which are commensurate it is possible to find a T for which all driving components have executed an integer multiple of their periods T_1 and T_2, in other words $mT_1 = nT_2$, for some integers m and n, and we set

$$T = mT_1 = nT_2.$$

In this case it is possible to define a net transport that depends on height above the plate only

$$W_{\mathrm{transport}}(z) = \int_0^T \left[-w_{\mathrm{sink}} + w_{\mathrm{swim}} H(|u_z(z(s),s)| - u_z^{\mathrm{critical}})\right] ds. \tag{6}$$

For a fixed value of the critical shear the net transport is thus a function of the ratio of the swimming speed to the sinking speed, or in other words, if

$$\beta = \frac{w_{\mathrm{swim}}}{w_{\mathrm{sink}}}. \tag{7}$$

then

$$\frac{W_{\mathrm{transport}}(z)}{w_{sink}} = \int_0^T \left[-1 + \beta H(|u_z(z(s),s)| - u_z^{\mathrm{critical}})\right] ds. \tag{8}$$

3 Results

3.1 Single Driving Frequency

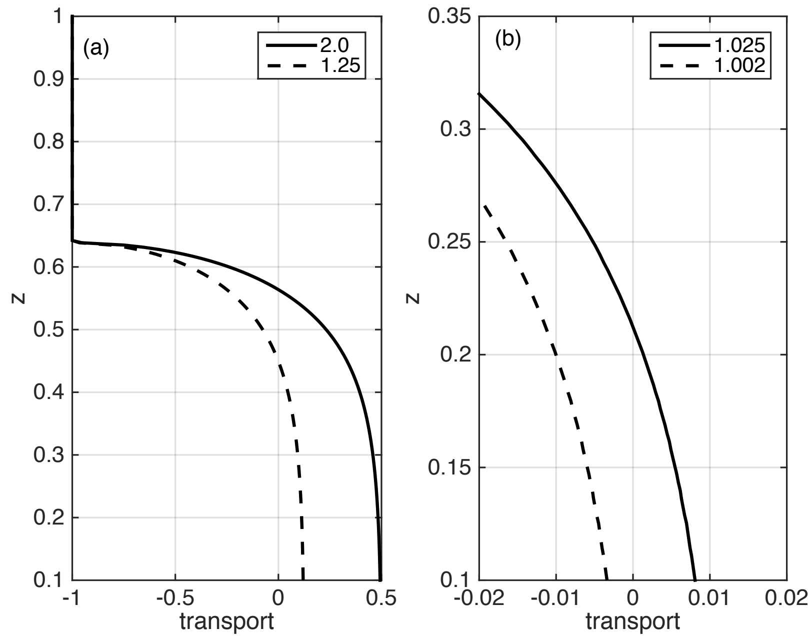

Figure 1: Net vertical transport for a single driving frequency case as β varies. For the left panel $\beta = 2.0$ (solid), and $\beta = 1.25$ (dashed). For the right panel $\beta = 1.025$ (solid), and $\beta = 1.002$ (dashed). Note for the dashed curve in the right panel there is no region of net upward transport.

In order for the particle to remain above the plate for all time, $\beta > 1$ is a necessary condition. Figure 1 demonstrates the structure of the net transport for various values of β in the single driving frequency case. The vertical coordinate has been scaled by the initial particle position and the net transport has been scaled by $w_{\text{sink}}T$ so that in the event of no swimming the transport will be equal to -1. When $\beta = 2$ net upward transport is evident for $z < 0.56$, while for $z > 0.64$ the shear is not sufficient to trigger any swimming. When β is decreased to 1.25, the region over which some swimming occurs, but is not strong enough to overcome the net downward sinking, grows to encompass $0.45 < z < 0.64$. For $z < 0.45$ a net upward transport is observed. Panel (b) shows values of β close to 1, where we note the different range of heights from panel (a). For the range of heights shown the case $\beta = 1.002$ never achieves a net positive transport. Despite the swim speed exceeding the sinking speed, the transport is downward at the heights shown. This means that the amount of time spent swimming is not enough to overcome sinking. Note also, that this result is dependent on keeping the strength of the harmonic driving fixed and a net upward transport could be achieved by increasing the amplitude of the plate motion.

The Eulerian transport results suggest that the limit cycles observed over a significant portion of parameter space are neither stable or unstable in the sense of ODE theory. Direct calculation confirms that for identical critical shears, different starting heights merely shift the limit cycles in the horizontal direction. Figure 2 shows an example. The initial height is varied by 5%, while all other the parameters are held fixed. It can be seen that the two limit cycles are translated copies of one another, and indeed a translation of the grey curve by 0.0132225 (derived at by trial and error computation) gives a maximum distance less than 10^{-6} between the two limit cycles. Thus the system, while simple to write down, is finely balanced in the sense that its phase space behaviour is complex, yet with a simple dependence on initial conditions. The remainder of the results section will explore some of the unusual properties that result when this precise balance is disturbed.

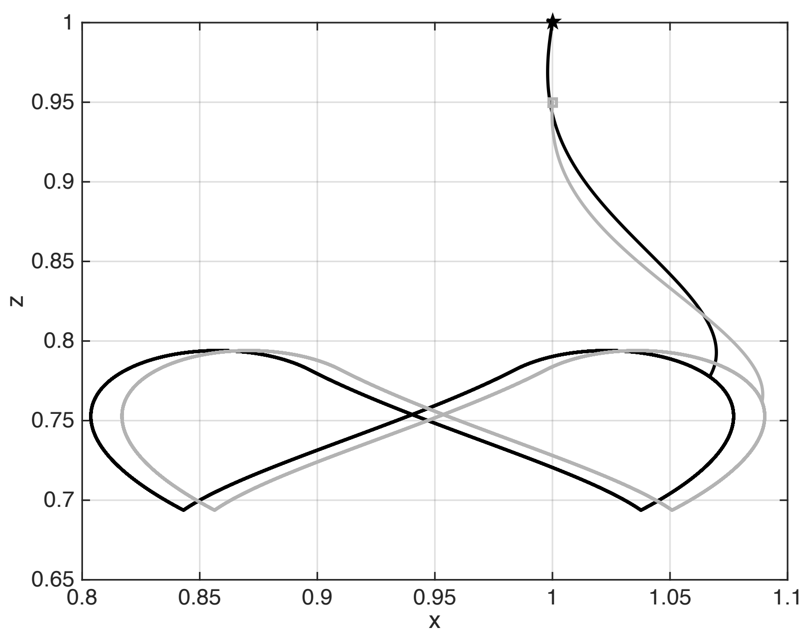

Figure 2: The effect of change in initial vertical position on the limit cycle. The symbols indicate initial position.

3.2 Multiple Driving Frequencies

The accompanying paper considered a single sinusoid driving frequency. We will now consider the two driving frequency case. The primary sinusoid has an amplitude of 1, and the perturbation sinusoid has an amplitude a_2. The form of the equation of plate motion is thus

$$u(z,t) = \cos(\omega t - mz)\exp(-mz) + a_2 \cos(\omega_2 t - m_2 z)\exp(-m_2 z), \tag{9}$$

with

$$m_2 = \sqrt{\frac{\omega_2}{2\nu}}.$$

It can immediately be seen that a lower perturbation frequency implies that fluid motion decays at a slower rate as one moves away from the plate.

3.2.1 Commensurate Frequencies: Net Transport

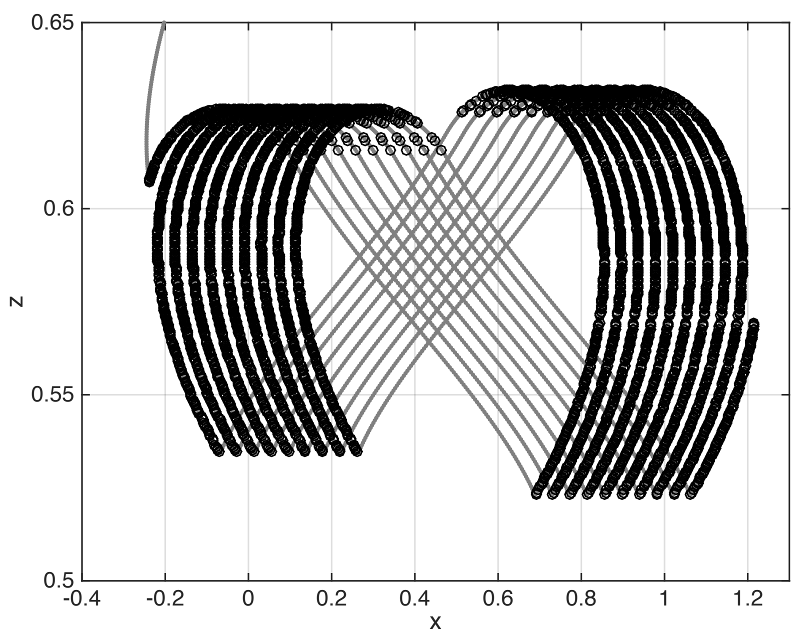

Figure 3: Perturbed limit cycle with drift. This is the $\omega_2 = 2\omega$, $a_2 = 0.2$ case for equation 9. Output times at which swimming is “On” are indicated by large black circles.

Figure 3 shows an example in which the perturbation frequency is double that of the primary frequency ($\omega_2 = 2\omega$) and the perturbation amplitude is 20% of the primary forcing ($a_2 = 0.2$). The ratio of the decay lengths exhibits a square root dependence and hence in this case $m_2 = \sqrt{2}m_1$. It is evident that unlike in the limit cycle, the two lobes differ in size (compare Figure 2). This size discrepancy is reflected in the mismatch between leftward and rightward advection, and leads to a net transport. It is also the reason why the figure appears to show several 'near' limit cycles. While an analogy may be drawn with Stokes drift [5], Stokes drift does not depend on swimming behaviour. We have found that any two commensurate frequencies we tried yielded net transport.

3.2.2 Incommensurate Frequencies: A More Complex Response

When the two driving frequencies are incommensurate, the precise balance that leads to the behaviour shown in Figure 3 is not observed and more complex behaviour can result. We consider a shear-triggered response to a primary driving frequency of $\omega = 2\pi/10 \approx 0.628$ perturbed by a secondary driving frequency ω_2. We investigate two perturbations: one having a lower frequency than the primary driving frequency, and one having a higher frequency. We will show that perturbations with a lower frequency ($\omega_2 < \omega$) led to the most complex phase portrait, albeit with no evidence of chaotic behaviour.

In Figure 4 we consider a case with a higher perturbation frequency $\omega_2 = 1 > \omega$, and a significant amplitude $a_2 = 0.5$. Despite the choice of a large amplitude for the perturbation, the phase portrait appears as a "smeared" version of the limit cycle shown in Figure 2. The time series of x and z in the upper right panel show a modulation, and this explains the smearing of the phase portrait. The base 10 windowed power spectra for these quantities, shown in the bottom panel, decay rapidly up to a frequency of around 8, with a set of packet–like peaks (albeit at much lower values) observed at high frequencies.

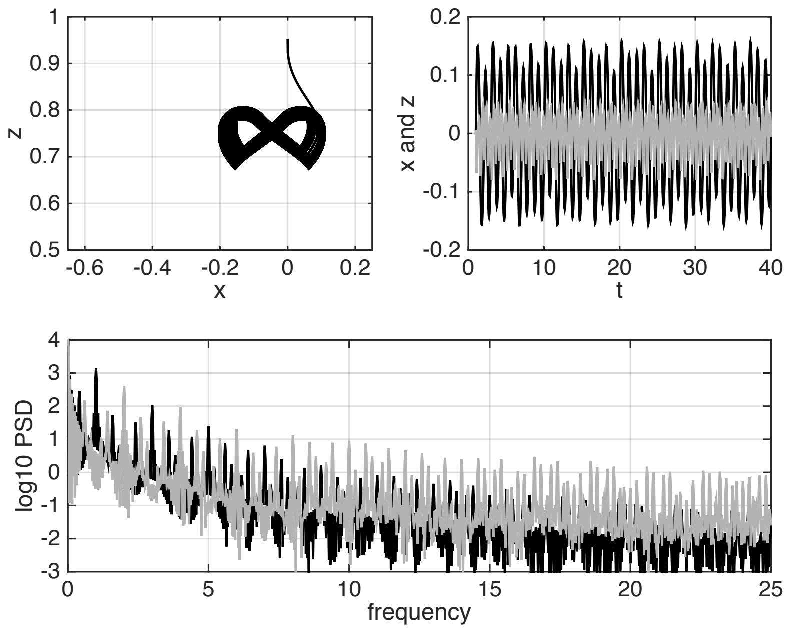

Figure 4: Two frequency driving $\omega_2 = 1 > \omega$, $a_2 = 0.5$. The phase portrait is shown in the upper left panel, the mean-centered time series of x (black) and z (grey) in the upper right panel and the power spectra of x (black) and z (grey) in the lower panel.

In Figure 5 we show the corresponding information for a lower frequency perturbation at a low amplitude, $\omega_2 = 0.5 < \omega$, $a_2 = 0.05$. The scales of the individual panels have been kept unchanged from Figure 4 to allow immediate comparison. It can be seen that the phase portrait is once again a "smeared" version of the limit cycle shown in Figure 2. Similarly, the time series of x and z show a modulation, but the power spectra decay exponentially, albeit with a more regular packet like structure of the various peaks.

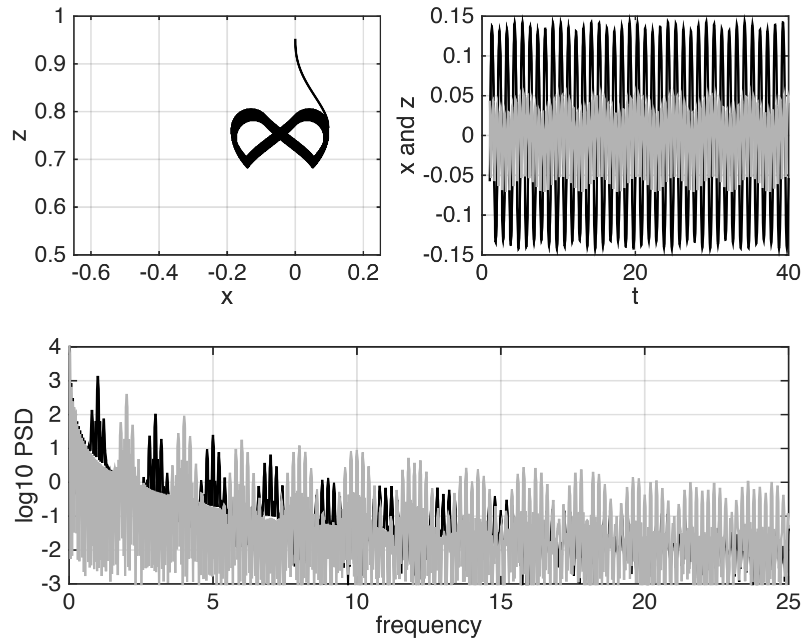

Figure 5: Two frequency driving $\omega_2 = 0.5 < \omega$, $a_2 = 0.05$. The phase portrait is shown in the upper left panel, the mean-centered time series of x (black) and z (grey) in the upper right panel and the power spectra of x (black) and z (grey) in the lower panel.

The response in the previous two examples is subtle. We systematically increased the amplitude of the perturbation for a low perturbation frequency case and discovered a much more pronounced response. Figure 6 illustrates this case, which has a perturbation driving frequency and amplitude given by $\omega_2 = 0.5$, $a_2 = 0.5$. The phase portrait shown in the upper left panel shows little resemblance to the tidy limit cycles of Figure 2, or their smeared counterparts in Figures 4 or 5. Nevertheless, we confirmed that variations in initial height still resulted in a phase portrait that was a horizontal translation of that shown in Figure 6. The motion thus does not exhibit an exponentially growing dependence on initial conditions, so the resulting behaviour is not chaotic.

As in its counterpart plots, the upper right panel shows the mean-centered time series of x (black) and z (grey). The base 10 logarithm of the windowed power spectra for these curves are shown in the lower panel. A fairly broadband spectrum is evident (for frequencies between zero and about five), with a stronger high frequency component for the z direction. This is sensible since this is the direction effected by swimming.

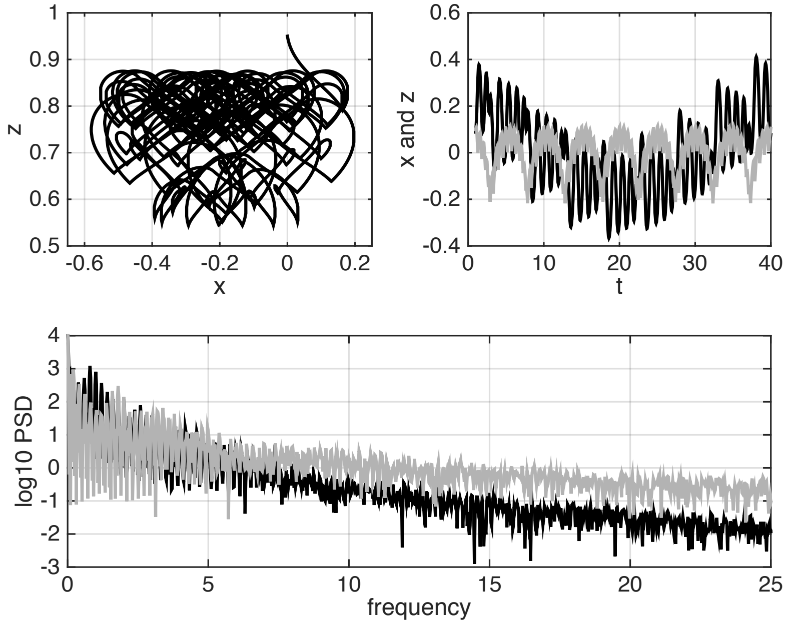

Figure 6: Two frequency driving $\omega_2 = 0.5 < \omega$, $a_2 = 0.5$. The phase portrait is shown in the upper left panel, the mean-centered time series of x (black) and z (grey) in the upper right panel and the power spectra of x (black) and z (grey) in the lower panel.

In order to quantify the transition from the "smeared" limit cycle to the more complex phase portrait shown in Figure 6 we computed a tiling fraction as a function of a_2 for both the low frequency and high frequency perturbations. We defined a rectangular domain that encompassed the phase portrait shown in Figure 6 using the maxima and minima x and z for the phase portrait. It was then tiled several different times using a different number of squares, where in each case we chose the same number of squares in each direction. A box was considered full if a trajectory passed through it, and $a_2 = 0$ corresponds to the tiling fraction of the limit cycle of the unperturbed case. For small numbers of boxes the measure is relatively insensitive to changes in the detail of a phase portrait. The sensitivity of the measure scales with the number of boxes used. This is shown consistently by the results shown in Figure 7. Panel (a) shows the low frequency case corresponding to the Figures 5 and 6. The tiling fraction can be seen to grow rapidly as the perturbation is introduced, even though its value remains below 0.2. For smaller numbers of boxes the tiling fraction saturates, while for the largest number of boxes the increase in tiling fraction continues up to about $a_2 = 0.4$ with an unexpected decrease thereafter. A visual comparison of the phase portraits resulting when $a_2 = 0.4$ and $a_2 = 0.5$ (not shown) suggests that the drop in tiling fraction with increased amplitude is the result of more tightly packed trajectories in the $a_2 = 0.5$ case. The high frequency perturbation case shown in panel (b) is qualitatively different with tiling fractions never reaching much beyond 0.2.

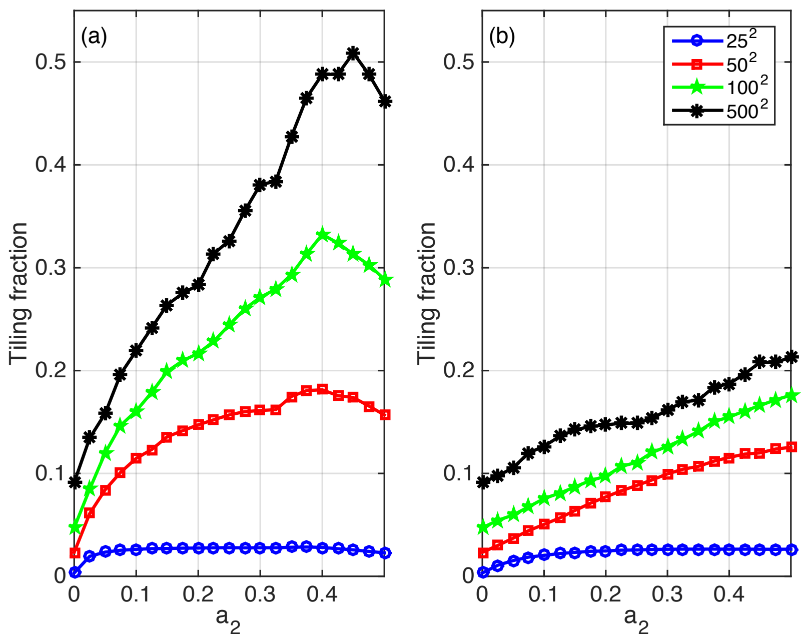

Figure 7: Tiling fraction as a function of a_2. (a) low frequency perturbation, (b) high frequency perturbation.

3.2.3 Eulerian Analysis of Transport

Because the Lagrangian response is manifestly nonlinear, while the governing fluid dynamics are linear, it is worth returning to the Eulerian transport analysis in order to compare vertical transport characteristics for the commensurate and incommensurate two frequency cases. In the case of incommensurate frequencies it is not possible to unambiguously define the T in (6) and the expression (5) must be employed instead. In Figure 8 we show the boundary between positive (below the curve) and negative (above the curve) cumulative Eulerian transport $W_{\text{cum}}(z, t)$ for two different perturbation frequencies. The base frequency is chosen as $2\pi/10$ and time is scaled by the corresponding period. Panel (a) shows two cases with $a_2 = 0.2$, and amplitude that is representative of the cases discussed above. While many different frequencies were investigated, for the figure $\omega_2 = 2\pi/5$ is shown in black and $\omega_2 = 4/3$ is shown in grey. The values were chosen so that one is irrational an the other rational, but both have a similar value. It is apparent that in contrast to the Lagrangian results reported above the Eulerian transport characteristics of the two cases are essentially identical. We systematically increased the amplitude of the perturbation driving, finding results consistent with panel (a) up to $a_2 = 0.6$. In order to demonstrate that the results actually do depend on the perturbation, panel (b) shows the results when $a_2 = 1$. At this extreme perturbation amplitude (indeed a semantic argument can be made that the perturbation should not even be referred to as a perturbation at this value of a_2) it is evident that some differences in cumulative Eulerian transport are observed. Nevertheless for perturbation amplitudes at which clear Lagrangian differences were observed (see for example the tiling fraction results in Figure 7) the Eulerian transport is largely unaffected by whether the perturbation frequency is commensurate with the driving frequency.

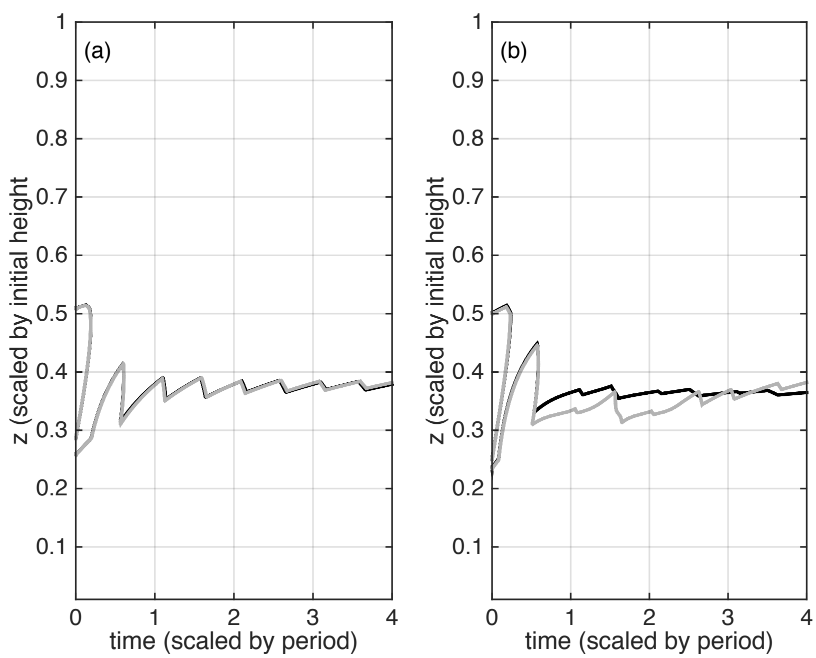

Figure 8: The boundary between positive (below the curve) and negative (above the curve) cumulative Eulerian transport $W_{\mathrm{cum}}(z,t)$. Both panels use the same perturbation frequencies: $\omega_2 = 2\pi/5$ (black) and $\omega_2 = 4/3$ (grey). (a) $a_2 = 0.2$, (b) $a_2 = 1$.

4 Conclusions

We have investigated the response and transport of swimming plankton subjected to hydrodynamic driving consisting of one and two frequencies. With a single driving frequency we find that when the upward swimming is triggered by a shear response, it is possible to have a net negative transport even when swim speed exceeds sinking speed (see Figure 1 b)). As pointed out in [6], if plankton swim and sink very slowly compared to the motion of the water, then they can basically be kept in suspension (even if the swimming speed is less than the sinking speed). Nevertheless, outside of this group we expect that many, if not most, would have a swimming speed much faster than their sinking speed. See for example Tables 1 and 2 in [7], which show that this is the case for the zooplankter *Calanus finmarchicus* in various stages of its development. Similarly Figure 2.15 of [6] shows that this holds for a variety of larger phytoplankton. This confirms the intuition that motile species which sink fast enough that they would not simply be held in suspension would require the ability to swim much faster than they sink. Otherwise, nearly constant swimming would be required to maintain vertical position, and vertical ascent would be very slow. This seems to impose an implausible energy output requirement, and would also make it difficult if not impossible to participate in daily vertical migrations. Therefore, we expect swimming speed to be much faster than sinking speed across a wide range of plankton species. We have shown that for shear triggered upward swimming this leads to net upward transport in our single driving case. More complex configurations would need to be considered on a case by case basis. The value of β for various species would require additional observations or experiments involving live plankton. It may be possible to rule out certain species having a shear response using an energy budget analysis. This is a candidate for future work.

We have found that for an oscillating plate a perturbation driving frequency that is commensurate to the primary one is enough to induce a systematic horizontal transport (Figure 3). This occurs due to a break in the symmetry of the limit cycle, with one side covering a systematically larger portion of phase space. An incommensurate perturbation driving frequency also broke symmetry but did so in a less systematic manner, meaning the limit cycle was "smeared" (Figures 4 and 5). For the case of a low frequency perturbation driving it was possible to induce complex phase space behaviour, with little resemblance to the original limit cycle (Figure 6). We explored the manner in which the transition to this complicated behaviour took place by tracking the tiling fraction for a portion of phase space, using a varying number of boxes to ensure the results were robust. We found that only low frequency perturbations led to tiling fractions over 0.3. More generally, it seems that lower frequency perturbations to the driving were most effective at separating limit cycle trajectories. The strength of the perturbation also tended to increase the area, but the tiling fraction was found to be a nonmonotonic function of the amplitude of the perturbation driving frequency. It may be that there is a similar phenomena when the perturbation frequency is lowered too far.

The above discussion is useful for several reasons. Swimming plankton models are quite easy to write down (for some examples see [2]), and relatively easy to include in software that has the capacity for Lagrangian particles. However, we have shown that the coupling of a simple swimming model and a very simple flow can lead to complex particle trajectories. This should serve as a cautionary tale that adding swimming plankton to more complex flows may lead to an explosion of complexity. This should not preclude the future construction of such models, but it does suggest that careful thought should be put into the design of tools to analyze their output.

It is quite likely that real organisms have a swimming response that is far less algorithmic than the simple model above, with the most obvious example being an intrinsic variability in the amplitude of the critical shear trigger across the population. As another example a constant β is an approximation. Clearly, plankton swim at more than one speed. Also some species of plankton are able to change their density [**?**]. This would change their sinking speed. We would therefore expect β to be a function of both time and space. Still, the sinking and swimming speeds can be interpreted as averages of the real quantities for modelling purposes, which was the approach we took here. The above described model and its results provide a basic building block with which a stochastic model can be analyzed. This is an obvious direction for future research.

Only two driving frequencies in superposition were considered here, but any number in superposition is possible. In this way any driving function may be chosen and approximated by a finite number of sinusoids in superposition. Clearly the analysis becomes much more complicated when the analysis moves beyond the "primary driving with perturbation" setup. However this also presents an opportunity. In many geophysical contexts the horizontal component of the flow dominates. If the flow in a plankter's habitat is known, it can be taken as the forcing function in the above model. By approximating β, the motion of the plankton could then be modelled near the bottom boundary layer. There are many opportunities for future work here.

We only examined a response to shear, but there are many more hydrodynamic characteristics which could theoretically act as cues for a biological response. In the accompanying paper, we considered a response to acceleration, but we could also consider a response to pressure, concentrations of dissolved substances, light intensity, turbidity, and temperature, to name but a few. These two works represent an attempt to systematically examine and quantify theorized biological responses to hydrodynamic stimuli. This requires a working knowledge of the scales and mechanisms of both the biological and hydrodynamic factors. For this reason this area of research is full of opportunities for interdisciplinary cooperation.

5 Acknowledgements

This work was supported by the Natural Sciences and Engineering Research Council of Canada through Discovery Grant RGPIN-311844-37157 to MS and RGPIN-386456-2010 to MW. Referee comments improved the clarity of the manuscript.

References

[1] Cartwright, J.E.H., Feudal, U., Károlyi, G., Moura, A., Piro, O. and Tél, T., Dynamics of Finite-Size Particles in Chaotic Fluid Flows. Thiel M., Kurths J., Romano M., Károlyi G., Moura A. (eds) *Nonlinear Dynamics and Chaos: Advances and Perspectives. Understanding Complex Systems*, page 51–89, 2010.

[2] Guasto, J.S., Rusconi, R. and Stocker, R., Fluid Mechanics of Plank- tonic Microorganisms. *Annual Review of Fluid Mechanics*, 44:373–400, 2012.

[3] Ianson, D., Allen, S.E., MacKas, D.L., Trevorrow, M.V. and Benfield, M.C., Response of Euphausia pacifica to small-scale shear in turbulent flow over a sill in a fjord. *Journal of Plankton Research*, 33(11):1679–1695, 2011.

[4] Kiørboe, T. *A mechanistic approach to plankton ecology*. Princeton University Press, 2008.

[5] Kundu, P.K., Cohen, I.M. and Dowling, D.R., *Fluid Mechanics: Fifth Edition*. Academic Press, Oxford, 2012.

[6] Reynolds, C.S., *The Ecology of Phytoplankton (Ecology, Biodiversity and Conservation)*. Cambridge University Press, Cambridge, 2006.

[7] Rudjakov, J. A., The possible causes of diel vertical migrations of planktonic animals. *Marine Biology*, 6(2):98–105, 1970.

[8] Shaw, J. and Stastna, M., A Model for Shear Response in Swimming Plankton. *Progress in Oceanography*, 151:1–12, 2017.

[9] Tschoegl, N.W., *The Phenomenological Theory of Linear Viscoelastic Behavior: an Introduction*. Springer Berlin Heidelberg, 1989.

Received January 2017; revised November 2017.

email: journal@monotone.uwaterloo.ca
http://monotone.uwaterloo.ca/∼journal/